Modular Lorentz Force Actuators for Efficient Biomimetic Propulsion of Autonomous Underwater Vehicles

by

Joseph Christopher Church

B.S., E.E. & M.E. M.I.T., 2013

Submitted to the Department of Electrical Engineering and Computer Science
in partial fulfillment of the requirements for the degree of

Master of Engineering in Electrical Engineering and Computer Science

at the

MASSACHUSETTS INSTITUTE OF TECHNOLOGY

June 2014

Signature redacted

Author .....
Department of Electrical Engineering and Computer Science
May 23, 2014

Certified by ..... Signature redacted
David L. Trumper
Professor of Mechanical Engineering
Thesis Supervisor

Signature redacted

Accepted by .....
Albert R. Meyer
Chairman, Masters of Engineering Thesis Committee

Modular Lorentz Force Actuators for Efficient Biomimetic Propulsion of Autonomous Underwater Vehicles

by

Joseph Christopher Church

Submitted to the Department of Electrical Engineering and Computer Science
on May 23, 2014, in partial fulfillment of the
requirements for the degree of
Master of Engineering in Electrical Engineering and Computer Science

Abstract

In this thesis, we developed a highly scalable design for modular Lorentz force actuators for use in segmented flexible-hull undersea vehicles such as the RoboTuna being developed at Franklin W, Olin College of Engineering. The actuators were designed to directly drive tail foil sections, or vertebrae, in an oscillatory motion to provide thrust. The design process was automated to facilitate implementation in different sized vertebrae. A set of prototype actuators was manufactured and tested to evaluate the feasibility of the design. A test stand was constructed to evaluate both the static and dynamic performance of the actuators. The prototype actuators achieved the required motion and demonstrated modest performance at a variety of load levels.

Thesis Supervisor: David L. Trumper
Title: Professor of Mechanical Engineering

Acknowledgments

There are certain people without whom this thesis would not have been possible.

I would like to thank

Professor David Trumper

Professor David Barrett

Phillip Daniel

Minkyun Noh

Jun Young Yoon

Lei Zhou

Roberto Melendez

Ian MacKenzie

Mark Belanger

Laura Zaganjori

Anne Hunter

Chris

Fiona

Mom

Dad

Will

Contents

List of Figures

List of Tables

Chapter 1

Introduction

1.1 Project Motivation

This project is motivated by the need for high efficiency propulsion of Autonomous Underwater Vehicles. Buoyancy requirements set strict limits on the amount of energy that can be stored in such vehicles. Traditional methods of underwater propulsion such as propellers offer limited efficiencies, further limiting the range of AUVs. The RoboTuna project, led by Professor David Barrett and his team at the Franklin W. Olin College of Engineering, has been exploring the use of oscillating foils (tails) as a means of propelling robotic fish (Figure 1.1). Their goal is to improve propulsive efficiency by mimicking the swimming techniques of fish. In addition to a potential increase in efficiency, their novel approach has another advantage: The RoboTuna blends in with its biological counterparts. The long term goal of the RoboTuna project is to develop less intrusive AUVs for studying ocean ecology and marine life.

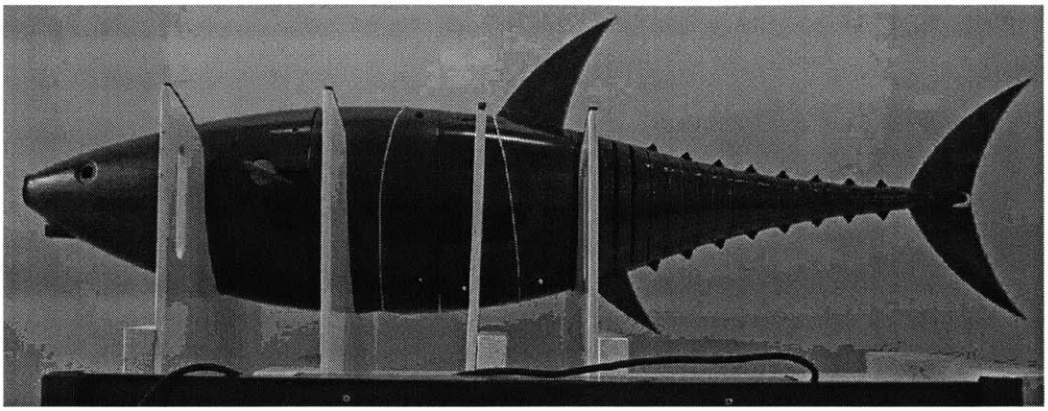

Figure 1.1: A recent RoboTuna prototype developed at Olin. Photo courtesy of Prof. David Barrett.

1.2 Summary of Work

Modular Lorentz force actuators were designed for Olin's RoboTuna. An appropriate actuator topology was carefully chosen and scripts were written for automated synthesis of actuator dimensions. A set of prototype actuators were then fabricated.

A test stand was designed and built for static and dynamic characterization of the prototype actuators. An actuator was characterized and compared to predicted performance. A second actuator was used as an active load for dynamic efficiency experiments.

1.3 Background and Prior Art

The RoboTuna project grew out of Professor David Barrett's 1994 PhD work on flexible hull underwater vehicles [1]. Early work demonstrated the improved efficiency of an oscillating foil over traditional propellers. While promising, the initial attempts were not self-contained. External actuators drove the tail sections via cables and pulleys. Since that time, researchers have been attempting to develop an efficient means of on-board propulsion. So far, this has proved challenging. Recent designs using high reduction gear motors and tendon-pulley transmissions have yielded relatively low efficiencies.

Currently, novel actuation schemes are being investigated to achieve the required slow oscillatory motion. Direct drive transmission from electromagnetic actuators is challenging due to their low efficiencies at low speeds. In 2013, Zhen Sun investigated a novel pulse drive system that would store mechanical energy from a pulsed EM actuator in an intermediate series elastic element [6]. This system allows the EM actuators to operate efficiently at high speeds while still delivering the required motion.

1.4 Scope Limitations

From its onset, this work has been limited to the development of a prototype voice coil type actuator for direct actuation of the RoboTuna's vertebrae. Numerous other actuation schemes were considered and set aside for future consideration. In particular, issues pertaining to swimming patterns, buoyancy, tail design, and waterproofing were explicitly not investigated. For the sake of generality, we chose to design a relatively simple actuator, taking note of possible areas where there might be room for improvement.

1.5 Goals

The goal of this research was to design, build, and characterize a set of prototype voice coil actuators to assess their potential for use in flexible hull AUVs. To this end, the actuator design was further constrained. The following requirements were set:

Size The actuators must fit within the vertebrae of a current RoboTuna prototype (Figure 1.2) and should be able to produce as much torque as possible within the size constraints.

Motion It was assumed that the desired motion of the vertebrae would be that of a simple harmonic oscillator. The actuators will drive the vertebrae at their natural frequency

and will thus see a purely dissipative load. They must be able to provide a $\pm 5^{\circ}$ range of motion.

Simplicity The importance of simplicity was twofold. A simple design would provide a baseline performance which could be later optimized. Additionally, a simple design would be easier to implement in hardware.

Efficiency Considerations From the onset we understood that high efficiency might not be achievable with direct drive voice coil actuation. However, we aimed to see what types of efficiencies might be possible. Wherever possible we would design for better efficiency.

Scalability The current RoboTuna prototype has 12 vertebrae, each potentially requiring two identical actuators. A modular design that could be scaled to fit each vertebrae would be highly desirable.

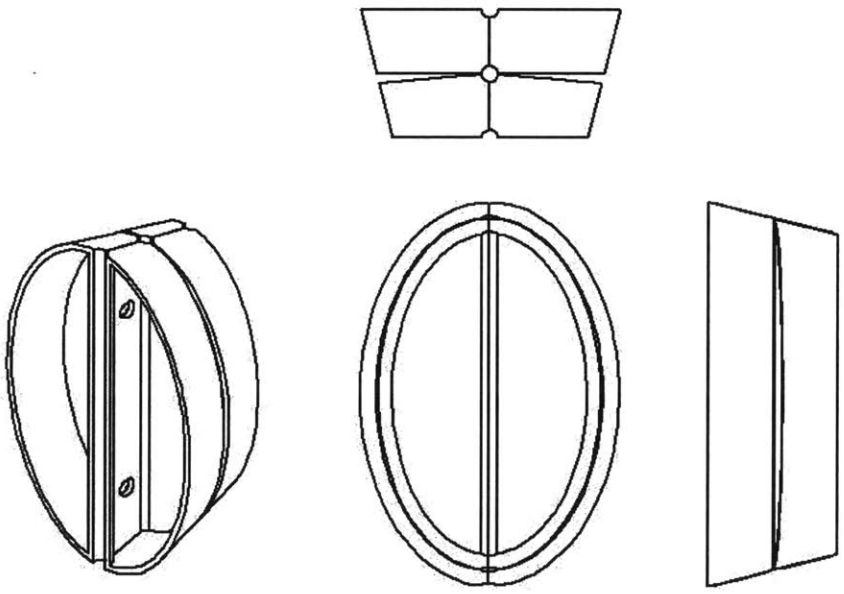

Figure 1.2: A pair of RoboTuna vertebrae

1.6 Thesis Structure Overview

The remainder of the thesis is structured as follows.

Chapter 2 details our design process. The efficiency of Lorentz force actuators is explored in detail. We discuss actuator topologies and develop automated design tools for our chosen structure.

Chapter 3 describes our prototypes. We discuss the manufacture of the actuators and present the finished prototypes.

Chapter 4 describes two tests that were performed to characterize the actuators: a static test for determination of the motor constant, and a dynamic test for determination of efficiency at various load levels. We present our test set-up, procedures, and results.

Chapter 5 discusses our results and reviews our work. We conclude this thesis and provide recommendations for future work.

Chapter 2

Actuator Design

2.1 Overview

The prototypes were designed to evaluate the potential of voice coil actuators as a means of efficient distributed propulsion. In our design process we aimed to distill out a solid baseline design rather than a highly optimized one. Our primary challenge was producing the required torques within the confined geometry of the RoboTuna's vertebrae. An initial efficiency analysis guided the entire process. The modular nature or the RoboTuna's tail inspired us to develop a scalable design for automated iteration.

2.2 Voice Coil Actuators

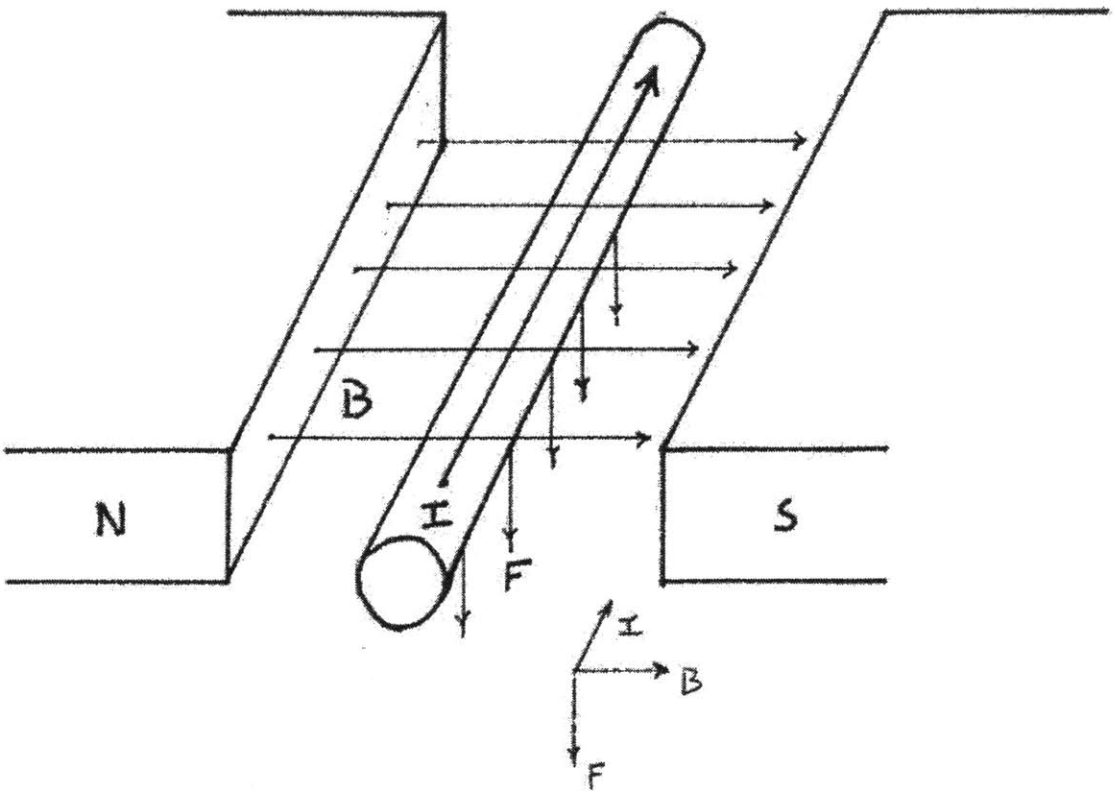

Figure 2.1: A simple Lorentz force voice coil type actuator.

A simple Lorentz Force actuator is shown in Figure 2.1. When placed in a magnetic field, a current carrying wire experiences a force as expressed by the second term in the Lorentz force law:

$$F = \int\int\int_V \rho E + J \times B dV \tag{2.1}$$

This effect is exploited in many types of electromagnetic actuators. A simple voice coil actuator is shown in Figure 2.2. Here, many turns of wire are placed in the magnetic field to multiply the effect. A well designed magnetic structure provides a strong uniform magnetic field. Such actuators are appealing due to their simplicity and linearity. They can

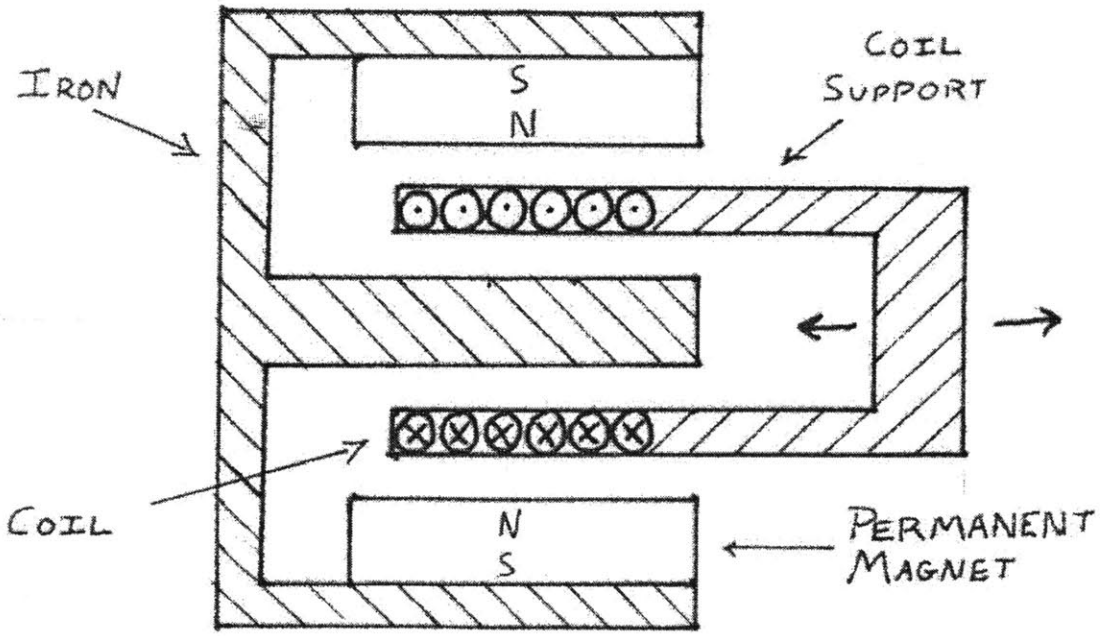

Figure 2.2: A simple voice coil actuator

be designed to produce either linear or rotational motion depending on their mechanical constraints. For a rotary actuator, the Lorentz force law can be approximated as

$$\tau = \iiint_V r \times (J \times B) dV = r n l_w I B_{eff} \,. \tag{2.2}$$

Here r is the moment arm, n is the number of turns, l_w is the length of the windings in the field, and B_{eff} is the perpendicular component of the magnetic field. Defining the motor constant k_m as the ratio of torque to current we find

$$k_m = \frac{\tau}{I} = r n l_w B \,. \tag{2.3}$$

Adding in the effects of winding resistance, R_w and winding inductance L_w, we can create a lumped parameter model for the ideal Lorentz force actuator as shown in Figure 2.3. Note that by energy conservation, the motor constant k_m determines the "back-EMF," E produced across the ideal transformer X. Conservation of energy requires

$$IE = \tau\omega \,, \tag{2.4}$$

and thus

$$E = \frac{\tau\omega}{I} = \frac{\tau\omega}{\tau/k_m} = k_m\omega \,. \tag{2.5}$$

This model captures all the primary characteristics of voice coil actuators. From this we can derive the static mechanical characteristics of the actuator. Additionally the $\tau_e = R_w/L_w$ electrical time constant is captured. For the remainder of this chapter we will assume that we are operating in electrical steady state, allowing us to neglect the presence of L_w.

For a given voltage, U, applied at the terminals of the actuator, the mechanical output is restricted to a torque speed curve like that shown in Figure 2.4. τ_s and ω_o are known as

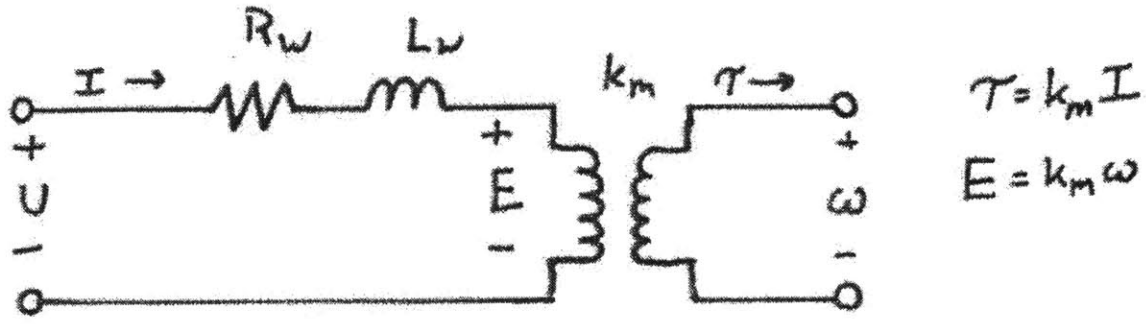

Figure 2.3: Electrical model of Lorentz force actuator

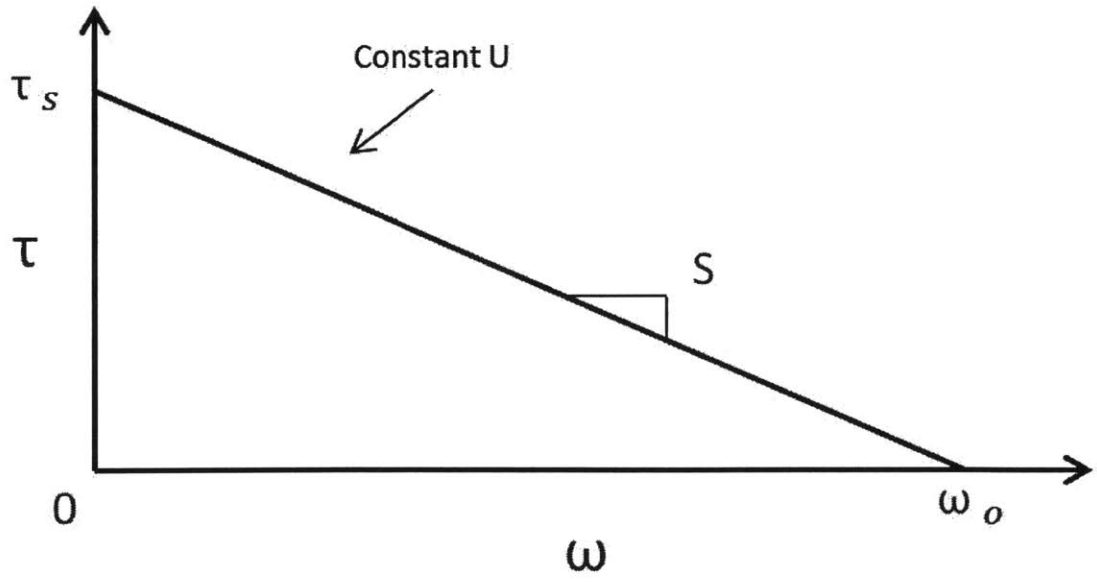

Figure 2.4: Torque speed curve

the stall torque and no-load speed respectively. The negative of the slope of this curve is an important characteristic of an actuator and is known as the motor's steepness, S [5].

We define τ_s as the torque produced when $\omega = 0$. Noting that when $\omega = 0$, $E = k\omega = 0$, we find

$$\tau_s = k_m I = k_m \frac{U}{R_w}. \tag{2.6}$$

Similarly, we define ω_o as the speed when $\tau = 0$. Noting that when $\tau = 0$, $I = 0$, we find

$$\omega_o = \frac{E}{k_m} = \frac{U - IR_w}{k_m} = \frac{U}{k_m}. \tag{2.7}$$

Taking the ratio of the two, we find an expression for S:

$$S = \frac{\tau_s}{\omega_o} = \frac{k_m^2}{R}. \tag{2.8}$$

2.3 Fundamental Efficiency Considerations

We define the efficiency of an electromagnetic actuator as

$$\eta = \frac{P_M}{P_E}. \tag{2.9}$$

Here $P_E = UI$ is the electrical power delivered to the actuator, and $P_M = \tau\omega$ is the mechanical power produced by the actuator. These terms are not generally equal since some power $P_{diss} = I^2 R_w$ is dissipated in the winding resistance. Rewriting η, we find

$$\eta = \frac{\tau\omega}{IU} = \frac{k_m \tau\omega}{\tau U} = \frac{\omega}{U/k_m} = \frac{\omega}{\omega_o}. \tag{2.10}$$

2.10 shows that for a given voltage U, the efficiency of a Lorentz force actuator is speed

dependent. It is important to note that ω_o is dependent on U and that the operating speed of the motor ,ω is dependent on the loading of the motor.

A little algebra allows us to rewrite η in another useful form:

$$\eta = \frac{P_M}{P_E} = \frac{P_M}{P_M + P_{diss}} = \frac{\tau\omega}{\tau\omega + I^2R} = \frac{k_m\omega}{k_m\omega + IR_w} = \frac{k_m}{k_m + IR_w/\omega} \cdots$$

$$= \frac{k_m/R_w}{k_m/R_w + I/\omega} = \frac{k_m/R_w}{k_m/R_w + \tau/\omega k_{m,}} = \frac{k_m^2/R_w}{k_m^2/R_w + \tau/\omega} = \frac{S}{S + \tau/\omega}. \tag{2.11}$$

Defining the ratio τ/ω as the mechanical impedance of the load driven by the motor, Z_{mech}, we can write:

$$\eta = \frac{S}{S + Z_{mech}} \tag{2.12}$$

In the case of an actuator driving a purely dissipative load, Z_{mech} is equal to the damping constant b:

$$\tau = b\omega \Rightarrow Z_{mech} = \frac{\tau}{\omega} = b \tag{2.13}$$

A single vertebra of the RoboTuna can be modeled as a rotational inertia, spring damper system with impedance

$$Z = \frac{Js^2 + bs + k}{s}. \tag{2.14}$$

Here J is the moment of inertia of the vertebra, k is the restoring spring constant of the RoboTuna's spine, b is the damping constant from viscous drag, and $s = j\omega$ is the Laplace variable. At the resonance frequency $\omega_o = \sqrt[2]{k/J}$, the impedance reduces to

$$Z(j\omega_o) = \frac{-J^2\omega_o^2 + jb\omega_o + k}{j\omega_o} = \frac{-k + jb\omega_o + k}{j\omega_o} = b \tag{2.15}$$

Thus, at resonance, the RoboTuna's vertebrae will appear as a purely dissipative load.

2.4 Implications

The above analysis gives a few key insights:

1. Lorentz force actuators are inefficient at low speed.

2. Efficiency is dependent only on a motor's steepness and the load it is driving.

For a given load level, high steepness means high efficiency. This also displays a fundamental limitation of direct drive Lorentz force actuators for use in robotics applications. η is equal to $\frac{\omega}{\omega_o}$, and for these applications, ω is generally low. However, this can be tackled via mechanical advantage: A gearbox or another means of mechanical advantage, such as a pulse drive system, can be used to drastically scale Z_{mech} [6]. For rotational motion, this could be as simple as increasing r. Such scaling allows us to deliver the same amount of power to the load, but at a more efficient region of the torque speed curve. For our purposes, we will stick to a direct drive approach, but will apply our force at the largest feasible radius within the fish body dimensions.

So, for high efficiency, we would like to maximize steepness, which is given by

$$S = \frac{k_m^2}{R_w} = \frac{(rnl_{eff}B)^2}{\frac{n\rho l_t}{A_{wire}}} = \frac{(rnl_{eff}B)^2}{\frac{n^2\rho l_t}{A_{total}}} = \frac{r^2 l_{eff}^2 B^2 A_{total}}{\rho l_t}. \tag{2.16}$$

Where l_{eff} is the length of the coil in the magnetic field (per turn), l_t is the total length of the coil (per turn), A_{wire} is the cross sectional area of the wire, A_{total} is the total winding area, and ρ is the resistivity of the wire. We see immediately that the number of turns, n does not effect the steepness. The l_{eff}^2/l_t proportionality suggests that we want to minimize the length of coil that is not in the magnetic field. Additionally we want a large coil cross

section A_{total}. But most importantly, steepness depends on r^2 and B^2. For high steepness, large r and B are low hanging fruit.

2.5 Current Density limits

While it does not play a direct role in determining efficiency, there is a fundamental limit on torque density of Lorentz force actuators. We cannot expect to be able to pump arbitrarily large currents through the coil due to ohmic heating, which can be quite substantial for large current densities. We can reasonably expect a maximum average current of around $5A/mm^2$ [3]. Of course, Higher peak currents might be acceptable, but higher average currents would require special cooling considerations.

2.6 Topology Selection

First, all possible actuator orientations were considered by taking a vector perspective. In order to get the maximum torque, the generated force must be tangential to the axis of rotation. Further, the magnetic field and the current should be perpendicular. This constrains the orientation of the windings and magnetic field. Figure 2.5 summarizes the possibilities.

For simplicity, only planar designs were considered. While it would be advantageous to have a gap that conforms to the outer surface of the vertebra, this would be harder to analyze and manufacture. This constraint reveals two possible configurations: horizontal and vertical fields (Figure 2.6).

The horizontal field has a few nice features. Due to the geometry of the vertebrae, a larger single actuator can be fit in this orientation. On the other hand, a vertical field design lends itself to stacking multiple modular actuators. Additionally, the horizontal field configuration has a single, relatively large radius, where in the vertical field design, torque is produced

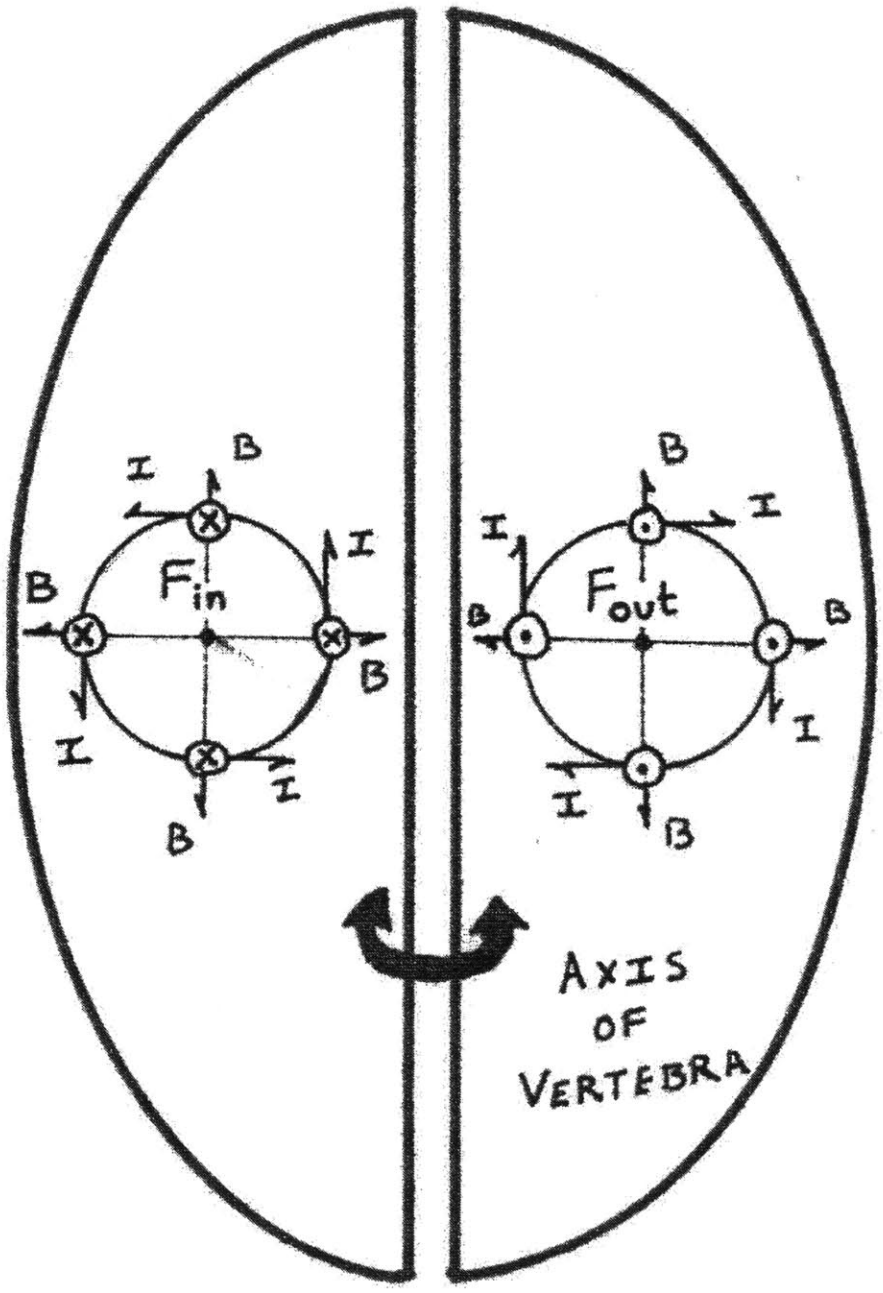

Figure 2.5: A vector perspective of the necessary forces.

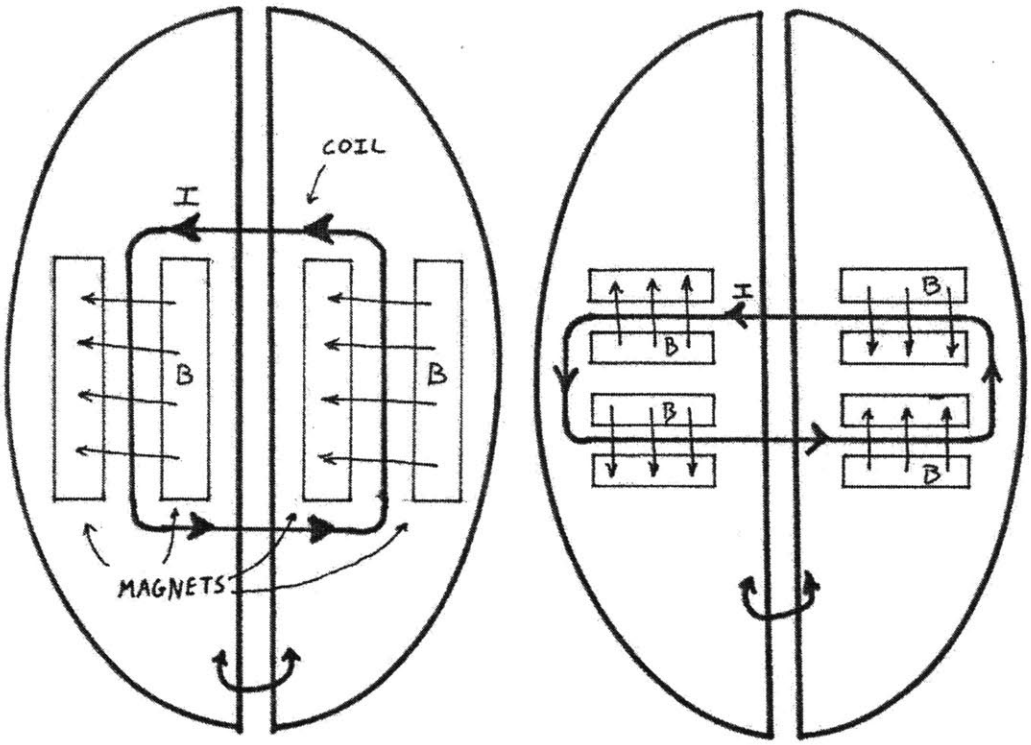

Figure 2.6: Horizontal and vertical field orientations

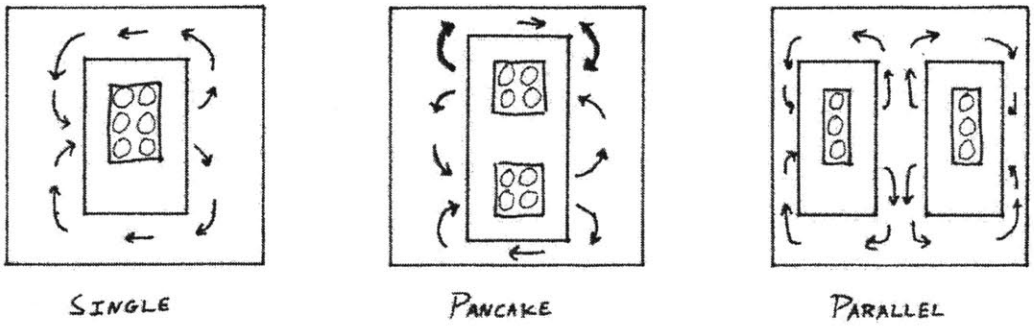

Figure 2.7: Horizontal gap topologies (cross section view from above).

along a radius.

Having settled on a horizontal field, more specific topological details were examined. Figure 2.7 shows the three primary topological concepts that we compared. The primary drawback of the "single" design is that it requires the winding to go from one side of the actuator to the other, resulting in a small $\frac{l_w}{l_t}$ ratio. Intuitively, this design's coil is not fully utilized as a large portion does not provide any torque. To its credit, it is potentially more compact and might allow for a flux focusing magnetic structure due to the saved space.

Of the two "double" designs, the pancake design is more appealing in that it has a larger average radius. Though slight, it is important since steepness is proportional to r^2. Unfortunately, The pancake design proved to be unfeasibly large given our required range of motion and our limited space. The parallel design was chosen for our prototypes.

2.7 Magnetics design

With a topology in hand, the magnetics could be designed. The goal here was attaining a high, uniform magnetic field in a small form factor. For this geometry, B_{gap} can be found as follows:

Consider the structure in 2.8.

From Maxwell's equations:

$$\nabla \times H = \mu_o(J + \frac{\partial E}{\partial t}) \tag{2.17}$$

$$\nabla \cdot B = 0 \tag{2.18}$$

The former, reduces to zero for our structure, as there are no currents (or diffusion currents) passing through the surface.

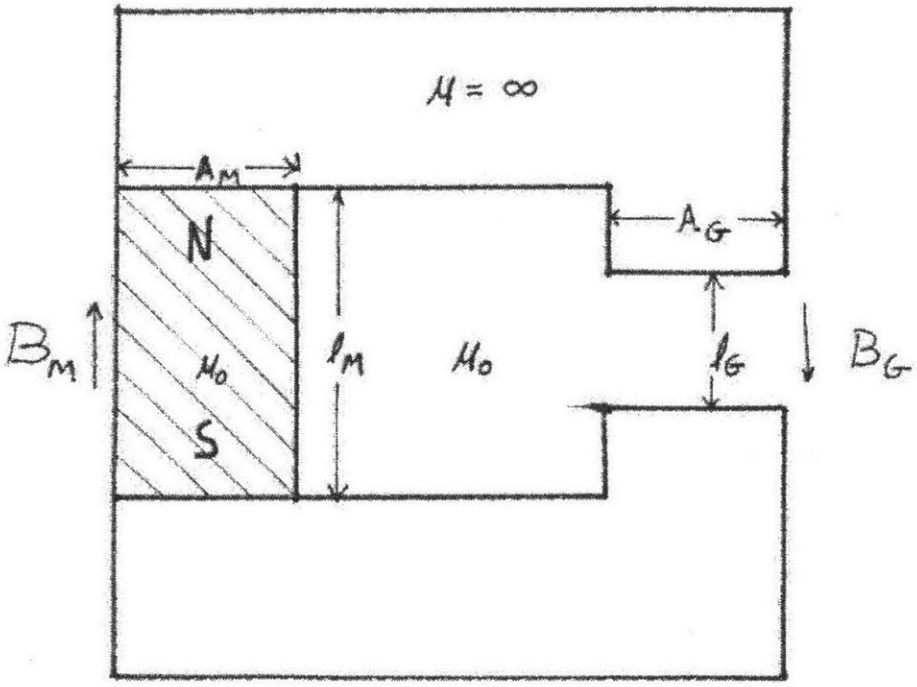

Figure 2.8: Simple magnetic structure

Together with the constitutive relation for the magnet, we can solve for the approximate fields (assuming uniform distributions, $\mu_{core} \gg \mu_o$, and neglecting fringing fields).

$$B_M = \mu_o(H_M + M) = \mu_o H_M + B_R \tag{2.19}$$

From 2.17 we can write:

$$H_M l_M + H_G l_G = 0 \tag{2.20}$$

From 2.18, we can write:

$$A_M B_M = A_G B_G \tag{2.21}$$

Combining these equations and solving for B_G, in terms of B_R and geometric constraints:

$$A_M(\mu_o H_M + B_R) = A_G(\mu_o H_G) \tag{2.22}$$

$$A_M\left(B_R - B_G\frac{l_G}{A_M}\right) = A_G B_G \tag{2.23}$$

$$B_R = B_G\left(\frac{A_G}{A_M} + \frac{l_G}{l_M}\right) = B_G\left(\frac{A_G l_M + A_M l_G}{A_M l_M}\right) \tag{2.24}$$

$$B_G = B_R\left(\frac{A_M l_M}{A_G l_M + A_M l_G}\right) \tag{2.25}$$

The above analysis holds for each half of the chosen topology.

Some notes on this result: For $A_m = A_G$,$l_M = l_G$, B_G will nominally equal $1/2B_R$. For a NdFeBr magnet with a $B_R = 1.2T$ this gives a $B_G = .6T$. This is a pretty good field

strength for a voice coil actuator. It is possible to get significantly higher values of B_G by increasing $\frac{A_M}{A_G}$ or $\frac{l_M}{l_g}$ or both. The former technique is known as flux focusing. While very appealing due to the $S \propto B^2$ relation, we decided not to pursue this route beyond paper designs for three reasons: 1) Flux focusing would require a significantly larger magnet and associated back iron and would be hard to fit in the vertebra. 2) Fields higher than around $1T$ would begin to noticeably saturate the back iron and would not increase B_G effectively. While iron has a B_{sat} of around $2T$, an average field of $1T$ could easily result in fields approaching$2T$ where the field is tightly confined within the back iron. 3) Complexity and associated loss of generality. The first two reasons also apply (to a lesser extent) to designs with $\frac{l_M}{l_g}$ greater than unity.

2.7.1 Automated Design

The above calculations formed the basis of a Matlab script that could generate dimensions for an actuator with a desired B_G given geometry constraints. The constraints included:

- maximum x, y, and z dimensions
- required angular range of motion
- margins between the coil and and the magnetic structure
- maximum magnetic field in the core given a uniform field approximation
- available magnets

The script returns a full set of dimensions for an actuator meeting the input constraints. A finite element model is automatically generated in FEMM to verify acceptable magnetic fields [4]. Additionally, the script automatically updates the dimensions of a SolidWorks model of the actuator.

The script allows a semi-automatic synthesis: It rapidly produces candidate designs given the designer's constraints. The designs it produces are not guaranteed to be practical and

are based on approximations. The designer must verify an acceptable gap magnetic field and check for saturation of the magnetic structure in FEMM. The script attempts to generate a design with the largest possible winding area, but ambitious constraints may return unacceptably small coil sizes. The designer must also verify that the generated design fits into the vertebra of the RoboTuna using the SolidWorks model.

2.7.2 Final Paper Prototype

The final prototype design was generated using the following Matlab input:

>>[P,R]=Actuator_Gen_lib_2(.6,.6,2,0,.02,1.5,MAGNETS);

The first three parameters are the maximum x, y, and z dimensions (in inches) of one half of the actuator. The next two parameters control the spacing between the magnets and the iron core in the y direction. If the first of these parameters is set to 1, Halbach magnets will be placed in this space. The second of these parameters sets the y dimension of this space. The next parameter is the radius of the center of the actuator. Finally, the last parameter is a set of magnet dimensions for the script to work with (see Appendix A for more details).

The following constants were set within the script:

magmargin= .02, arclength = 12 degrees, Br = 1.32, Bcsat = 1.5

Here,"magmargin" is the nominal clearance between the coil and the magnets, "arclength" sets the angular range of travel of the coil, "Br" is the remnant field of the magnets, and Bcsat sets the maximum acceptable B field in the core as calculates using the above approximations.

The resulting FEMM model is shown in Figure 2.9, and the magnitude of the horizontal B_G field component along the center of the gap is shown in Figure 2.10. The FEMM model includes the magnetic material properties of the magnets, iron, and air.

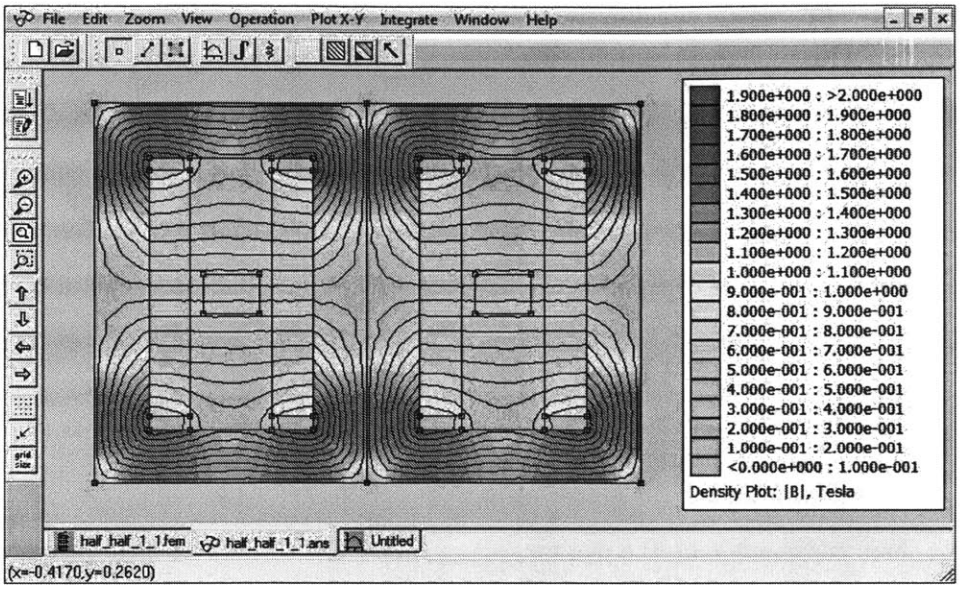

Figure 2.9: FEMM model of actuators

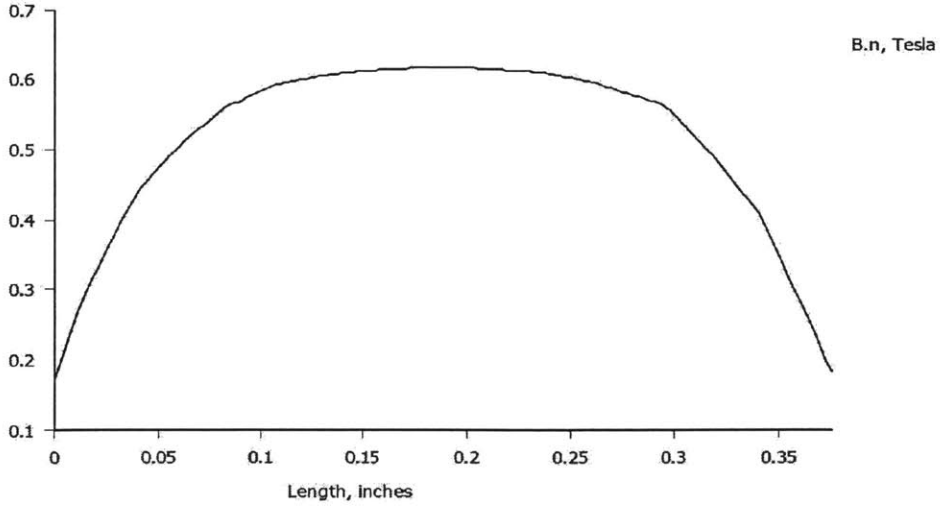

Figure 2.10: B_G along the center of the gap

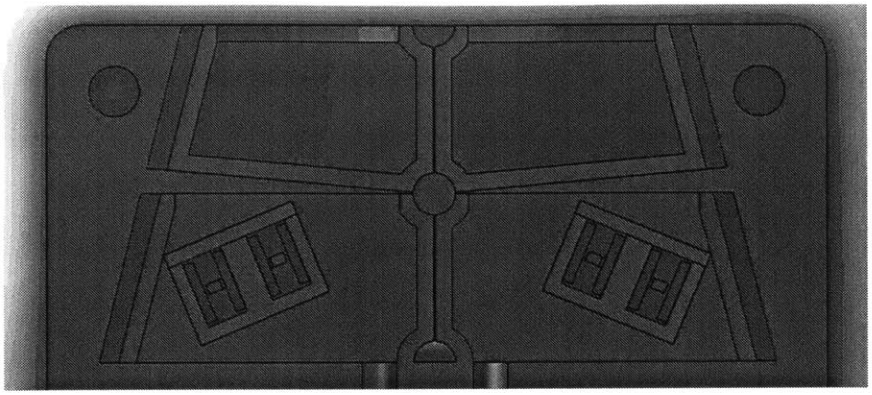

Figure 2.11: SolidWorks from Matlab script

The solid model generated is shown in Figure 2.11,

The final dimensions are shown in Figure 2.12. The structure extends 2" into the page.

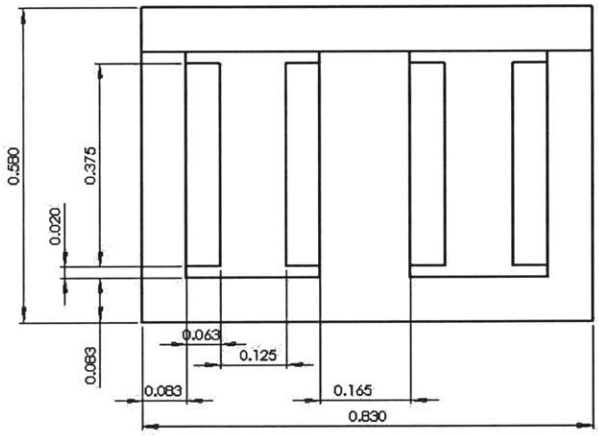

Figure 2.12: Actuator dimensions (inches)

2.8 Coil Design

The critical winding dimensions were generated using the Matlab script. The tradeoff between number of windings, n and wire gauge was left as a free parameter. It does not effect the steepness of the actuator as long as the effective winding cross section remains the same. Wire gauge can be chosen to match the coil to a power supply, or to ease manufacturing of

the coils.

2.9 Summary

To summarize, we taylored a set of voice coil type Lorentz force actuators to fit within the vertebrae of Olin's RoboTuna. Our design process was grounded in fundamental efficiency considerations, and grew into a script that could rapidly generate candidate designs based on our chosen topology. The next step is to build a set of prototype actuators.

Chapter 3

Hardware Realization

3.1 Overview

Two prototype actuators were manufactured for testing and verification of the design. First we describe the construction of the prototypes, making note of difficulties encountered while winding the coils. We then present photos of the final prototypes. Finally, the electrical characteristics of the coils are measured and performance of the actuators is predicted.

3.2 Actuator Magnetic Structure

The magnetic structure was broken into two pieces, an "E" and "I" core, to ease manufacturing and assembly. They were machined from ASTM A247 gray cast iron. Machining the "I" core was particularly difficult due to its thinness. An initial attempt resulted in a "potato chip" effect due to warping. One notable departure from the paper design was the addition of small steps in the E core to ease assembly (Figure 3.1). The magnets were then very lightly coated with Aero Marine #300 epoxy and carefully placed in their final locations. Great care was taken to avoid catastrophic collisions and improper orientation of the magnets.

Figure 3.1: Before and after: The magnetic structure was machined from cast iron stock. Note the small steps in the bottom corners of the slots.

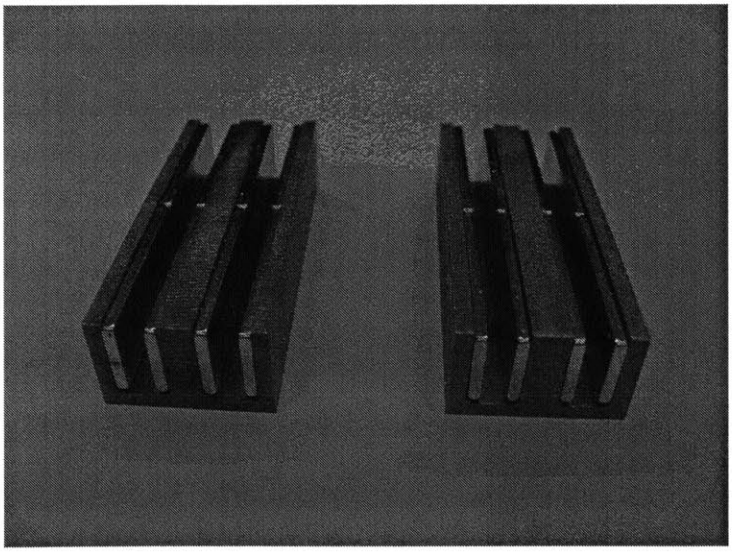

Figure 3.2: The E cores with magnets epoxied in place.

3.3 Actuator Coil

To form the coils, enamel coated magnet wire was hand wound around a rotating mandrel and coated in epoxy. The mandrel was designed with a sandwich structure to ease removal of the finished coil (Figure 3.3). The removable end pieces were designed to double as mounting brackets for the coil.

Winding the proposed coil posed some interesting challenges. In order to maximize the actuator's steepness, S, the windings must be packed as densely as possible. In theory, round wires can be optimally packed in a hexagonal grid to fill a plane achieving a density of $\frac{\pi}{\sqrt{12}}$ or 90.69% [2]. If the coil cross section is large compared to the cross section of the wire, hexagonal packing will approach this density. However, this so called "perfect packing" is not necessarily the densest when we consider coils in which the wire diameter is comparable to the dimensions of the coil. Packing arrangements were compared in Matlab for a variety of different wire gauges (Figure 3.4).

After winding a few test coils it became apparent that the long straight geometry of the coil would make any uniform packing difficult to achieve. The windings had a tendency to bow outward along the length of the coil. Successive layers compounded the issue until about the third layer, at which point new windings would slip into lower layers and the lattice structure was lost. About six coils were made with various gauges of wire. The best two were constructed with $26AWG$ wire, and had 13 turns and 10 turns each. Their respective densities were 51% and 39%.

3.4 The Prototypes

Here are the final two actuators. One would be used for characterization of the actuator (FUT), and the other as an active load driven against the FUT.

Figure 3.3: The coil mandrel

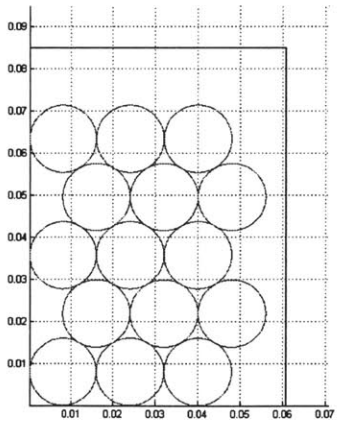

Figure 3.4: One possible filling with 26 AWG wire.

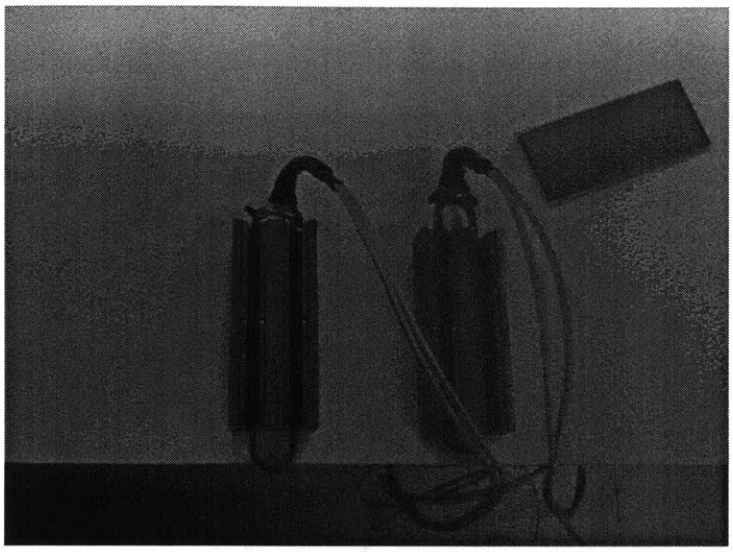

Figure 3.5: The final prototypes (only 1 "I" core shown)

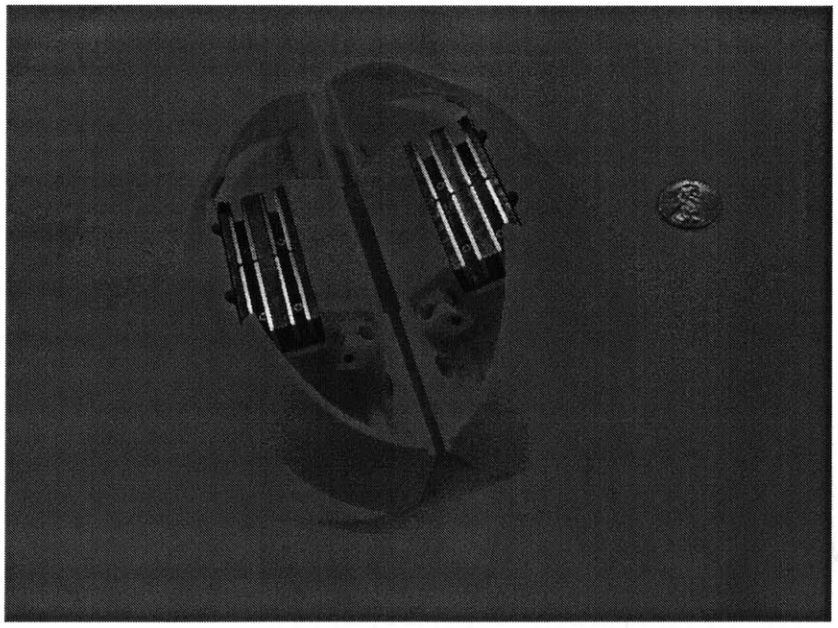

Figure 3.6: The stators

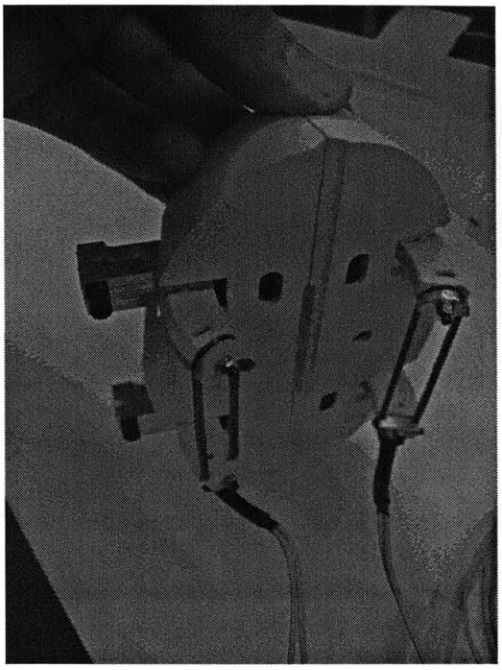

Figure 3.7: The rotors

3.5 Expected Results

Here we summarize the expected performance of the prototype actuator under test.

Since the prototype coils did not quite match the design specifications, their electrical characteristics were determined empirically using an impedance analyzer3.1.

coil	n	R_W	L_W@100Hz
Load	10	.234Ω	$26\mu H$
FUT	13	.267Ω	$37\mu H$

Table 3.1: Electrical characteristics of prototype coils.

The expected values were computed as follows. These estimates are optimistic as they assume a uniform B field of $0.6T$.

r_{avg}	$31.1mm$
n	13
l_w	$2 \times 50.8mm$

Table 3.2: Factors in calculation of k_m

$$k_m = rnl_wB = (0.0311m)(13)(.1016m)(0.6) = .0246N \cdot m/A$$

$$S = \frac{k_m^2}{R_w} = 0.00227\frac{N \cdot m \cdot s}{rad}$$

$$\eta = \frac{S}{S + Z_{mech}}$$

n	13
$k_m(\frac{N \cdot m}{A})$	0.0246
$S(\frac{N \cdot m \cdot s}{rad})$	0.00227
$\eta@Z_{mech} = 0.091(\frac{N \cdot m \cdot s}{rad})$	2.4%
$\eta@Z_{mech} = 0.050\ (\frac{N \cdot m \cdot s}{rad})$	4.3%
$\eta@Z_{mech} = 0.012\ (\frac{N \cdot m \cdot s}{rad})$	16%
$\eta@Z_{mech} = 0.0067\ (\frac{N \cdot m \cdot s}{rad})$	25%

Table 3.3: Expected k_m,S,η for the FUT

Chapter 4

Testing

4.1 Overview

A test stand was designed and constructed in order to characterize the actuators. Two tests were performed to evaluate the prototypes: a static test to measure the motor constant, and a dynamic test to demonstrate the achieved dynamic efficiency.

4.2 Test Stand Design

A test stand was designed around a current RoboTuna CAD model. A single joint created by the two largest vertebrae would form the basis for the test stand. The vertebrae were modified to accommodate a single set of prototype actuators and the required sensors.

The larger of the two vertebrae would act as a stator, housing the magnetic structure of the actuators. The second vertebra would act as a rotor, supporting the actuator coils within the magnetic structures. The vertebrae were linked by a "spine" flexure. Additional weights were added to the free vertebra to increase the moment of inertia so that the resonant frequency would be similar to that expected in a full size RoboTuna. The design for the flexible spine was taken directly from the existing RoboTuna CAD model and cut out of 0.005" stainless steel on a waterjet. Load cell mounting hardware was machined out of aluminum. Standard

fasteners were used. All sensors were read into Labview using a National Instruments PXI-6259 multifunction DAQ.

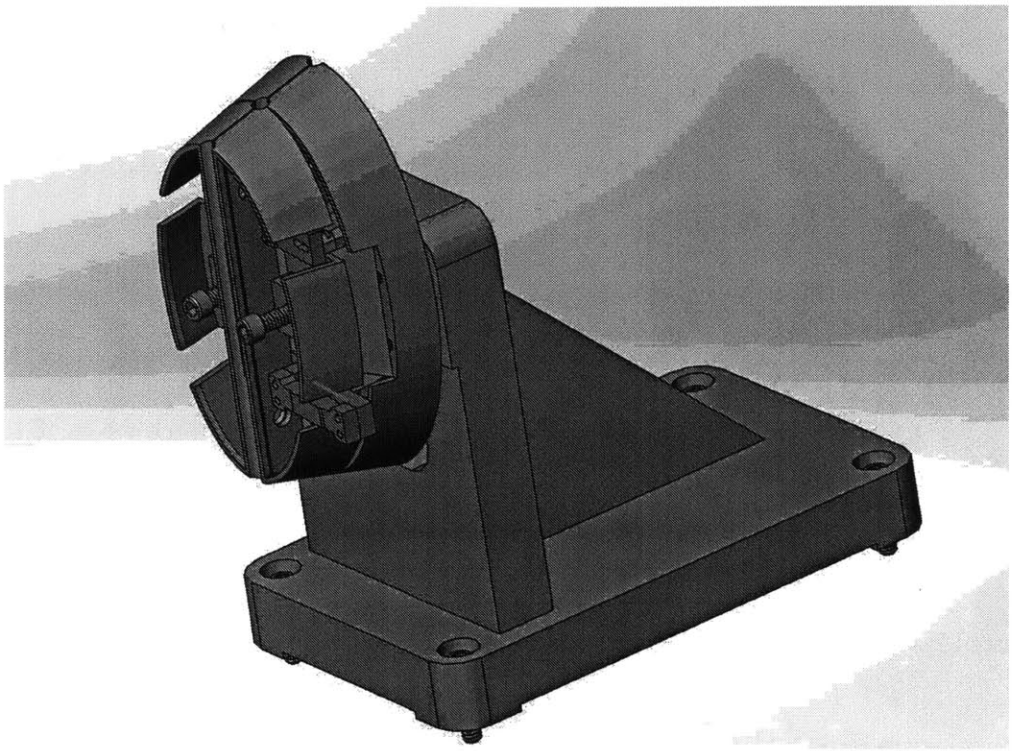

Figure 4.1: CAD model of the test stand

4.2.1 Load Cells

Two parallel beam load cells similar to those used in electronic scales were designed into the test stand to measure the torque produced by the primary actuator. They were installed at either ends of the primary winding between the coil mounts and the free vertebrae (Figure 4.3). INA128 instrumentation amplifiers were used to amplify the strain gauge bridge output voltage.

The load cells were purchased as surplus and required individual hand calibration. After locking the free vertebra in place, a constant force was applied to each load cell using a force gauge. Offset and scaling factors were then applied in Labview and were tuned until the

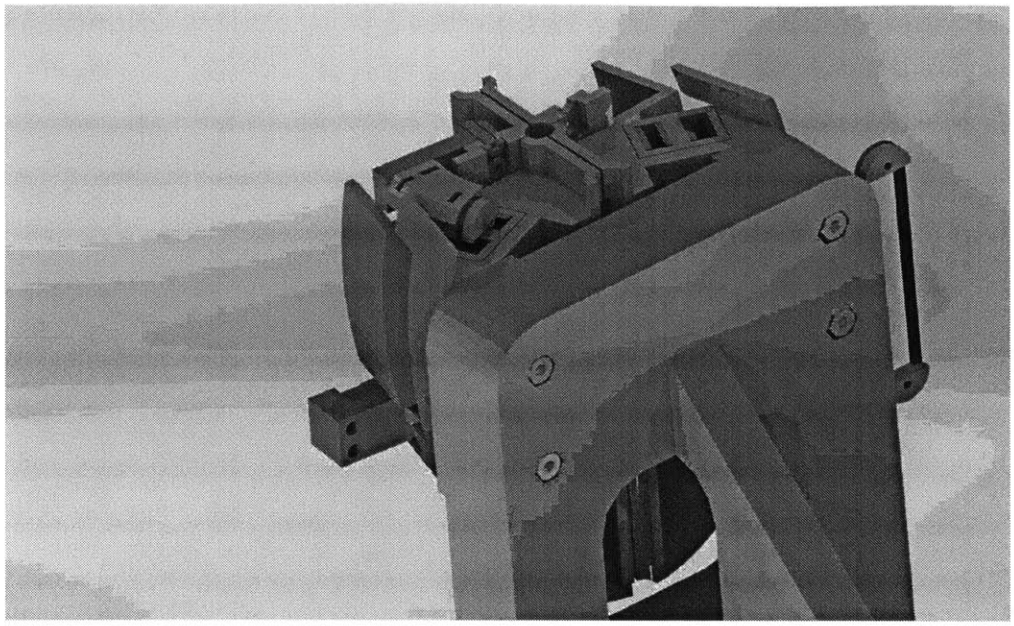

Figure 4.2: A cross section rendering of the test stand

adjusted load cell readings matched the force gauge.

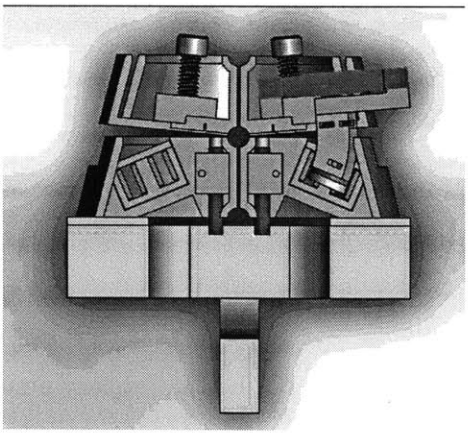

Figure 4.3: Load cell placement

4.2.2 Eddy Current Sensors

Kaman DIT-5200 eddy current position sensors were designed into the test stand. They were placed according to the manufacturer's recommendations in a differential configuration

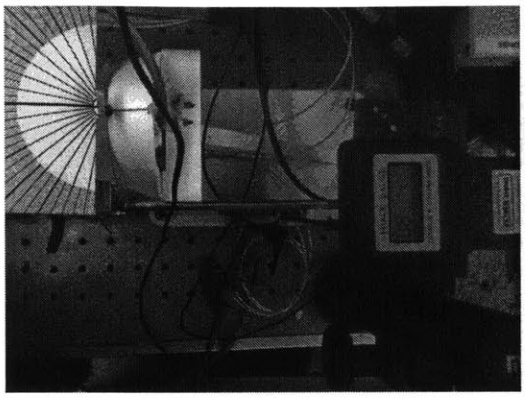

Figure 4.4: Load cell calibration

(Figure 4.5). Aluminum targets measuring roughly 0.5" × 0.75" × 0.03" were designed into the free vertebra, and mounting clamps were designed into the body of the fixed vertebra.

The Kaman DIT-5200 eddy current position sensors were calibrated to within .5°using the simple set up shown in 4.6. A small mirror was fixed to the free vertebra and a laser was reflected off of the mirror onto a protractor. The angle of the free vertebra was found by dividing the angle read off of the protractor by two. The probes and their targets were installed according to the manufacturer's instructions. The sensor's raw output was then scaled to match the angle measured using the laser and protractor.

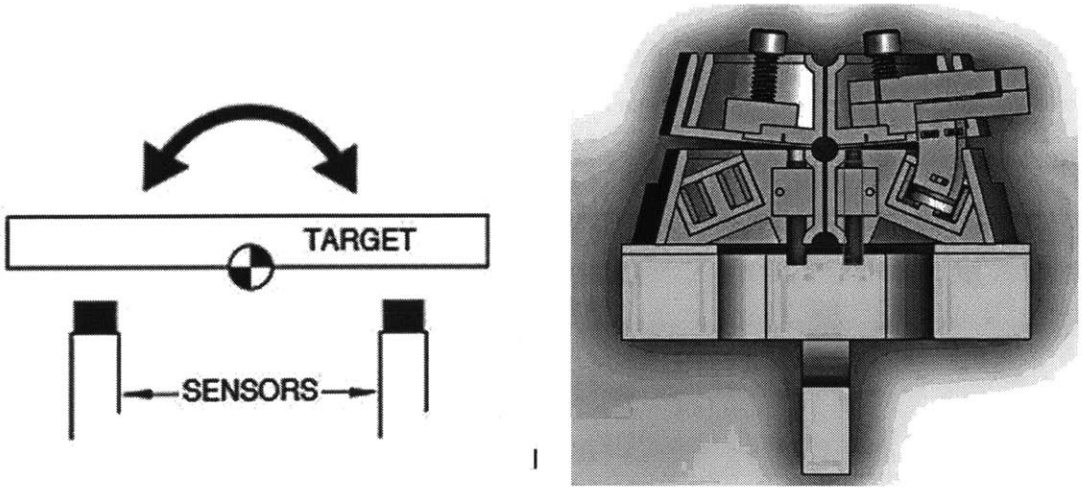

Figure 4.5: Eddy current probes in differential configuration

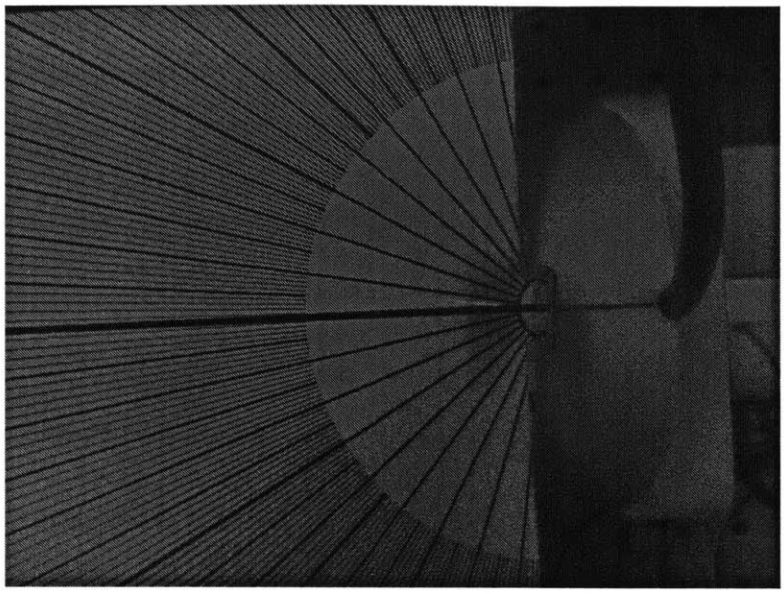

Figure 4.6: Angle calibration

4.3 Static Test

4.3.1 Setup

To measure the motor constant the free vertebra was simply locked in place using built-in set screws. Fixed currents were then driven through the actuator under test. The resulting torques were then measured via the load cells, and the motor constant was computed. This was repeated for various current levels and relative angles to test for current saturation and to check the uniformity of B_G.

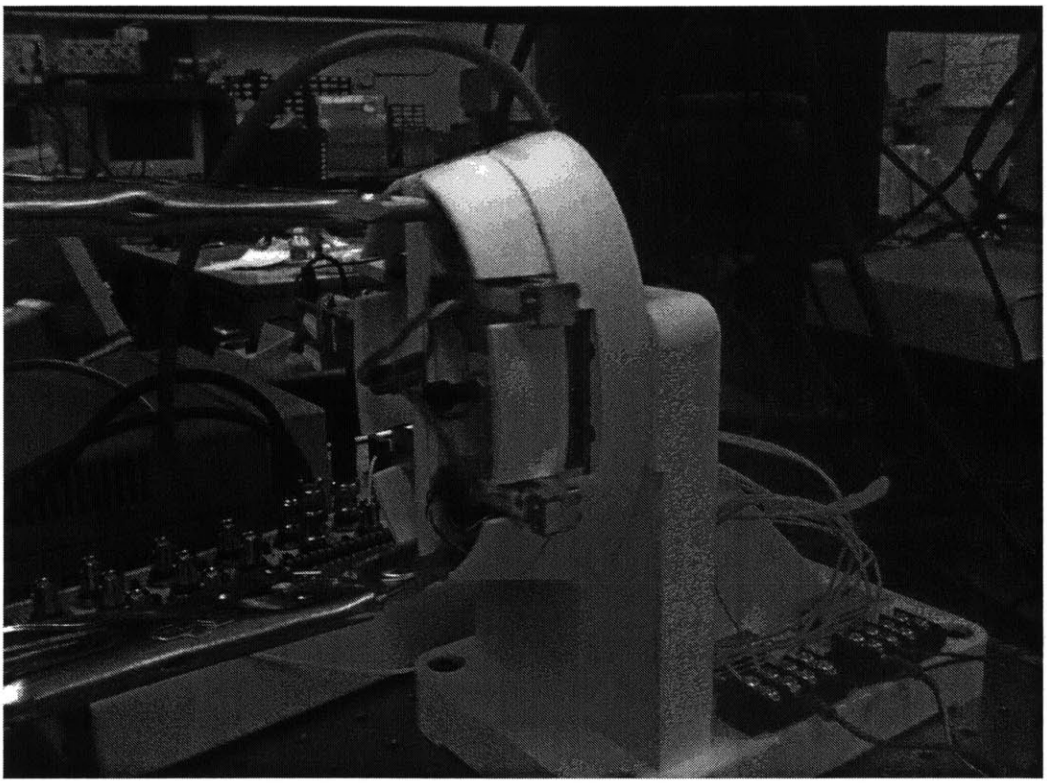

Figure 4.7: The test setup

4.3.2 Results

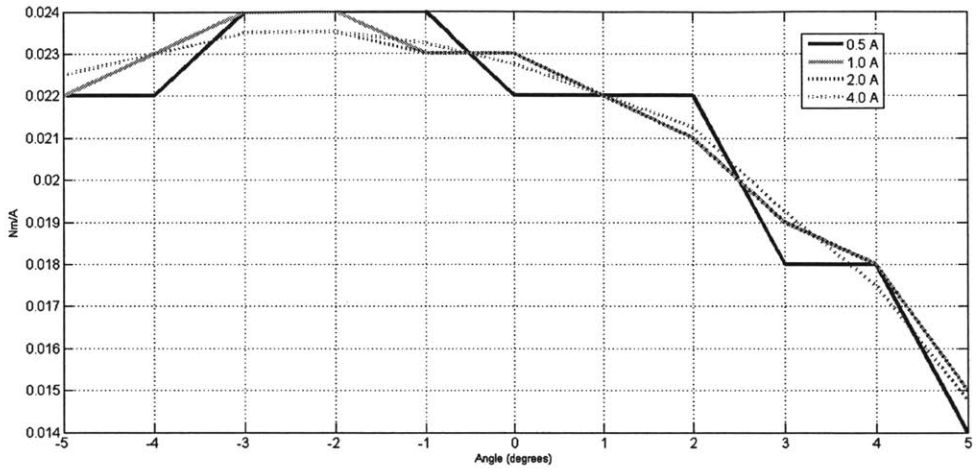

Figure 4.8: K vs theta at various current levels

4.4 Dynamic Test

While the motor constant and the winding impedance fully characterize the actuator, we felt it important to demonstrate dynamic efficiency. An adjustable viscous load was implemented using the second actuator and an impedance control loop. Due to time constraints, we were only able to run preliminary tests with this setup.

4.4.1 Setup

For this test, the actuator under test was used to drive the free vertebra at resonance at a fixed amplitude or 4°. A second actuator was used as an active damper. A control loop from θ to i allowed us to vary the effective damping. Since all tests were done at resonance, adjusting i to maintain a constant amplitude allowed us to vary load levels. θ, τ, I and U were measured and used to compute power in, power out and efficiency.

4.4.2 Active Damper

An impedance control loop was used to provide an adjustable viscous load. A block diagram of the active damper is shown in Figure 4.9.

The impedance control loop was implemented in Labview using a NI myRIO. The controller was designed using continuous time transfer function blocks and run in a $10kHz$ Control Design and Simulation loop. A PI controller was implemented in a minor loop to provide current control. The loop was empirically tuned to provide adequate tracking and stability. An outer impedance control loop was designed to provide derivative action from θ to i_{ref} at low frequencies. A second order low pass filter was implemented at $16Hz$ in order to provide stability over a range of gains and to attenuate noise at high frequencies.

For each value of the damping gain, the vertebra was tuned to resonance. Z_{mech} was measured by taking the ratio of the torque output to the angular velocity of the vertebra. P_M and P_E waveforms were generated in Labview, and the rms efficiencies were computed with the collected data.

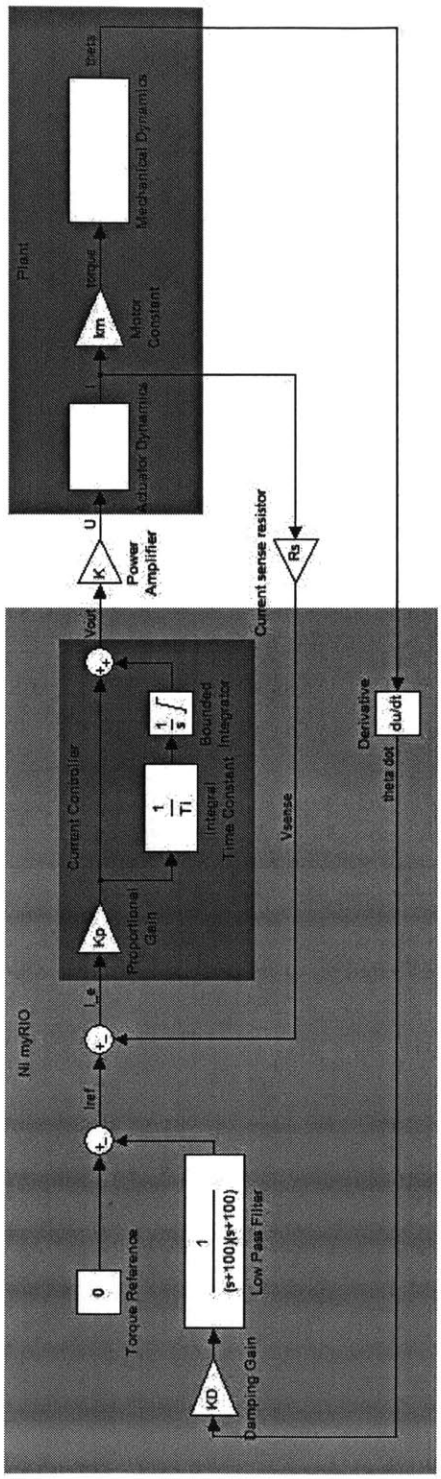

Figure 4.9: Active damper block diagram

orientation

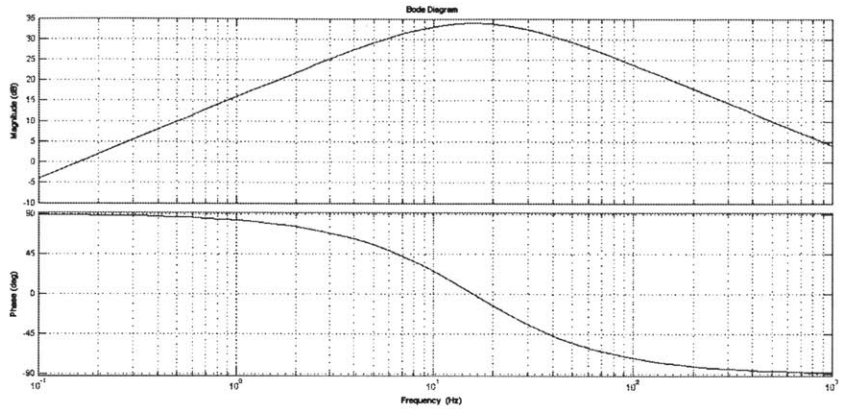

Figure 4.10: Bode plot damping of controller

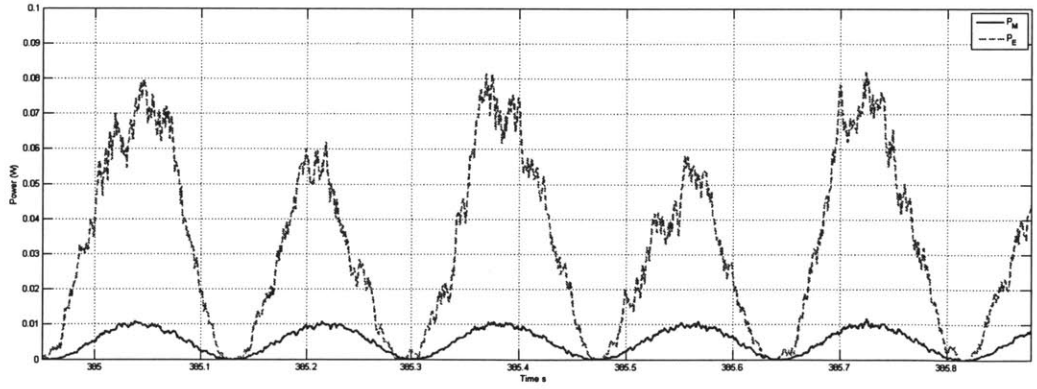

Figure 4.11: An example of the measured power waveforms

4.4.3 Results

Approximate Load Level Z_{mech} $(\frac{N \cdot m \cdot s}{rad})$	rms efficiency
0.091	1.4%
0.050	2.3%
0.012	10%
0.0067	16%

Table 4.1: Rms efficiency at various load levels

Chapter 5

Conclusions and Suggestions for Future Work

5.1 Discussion of Results

The measured values of the motor constant k_m closely matched the expected value given the achieved number of turns in the coil. Taking a closer look at the factors that determine k_m can give us some insight into the performance of these actuators. To reiterate:

$$k_m = rnl_wB \tag{5.1}$$

r,n, and l_w are all constant and known (Table 3.2). Thus, our experimental measurements of k_m reveal the effective magnetic field B.

This graph confirms that we achieved a magnetic field greater than $0.5T$ over much of the gap. As expected, the field falls off near the ends of the range of motion. While very similar to Figure 2.10, this plot shows the measured effective B field along the true path of the windings, not along a straight line through the center of the gap. A slight misalignment of the coils could explain the asymmetry in the measured field.

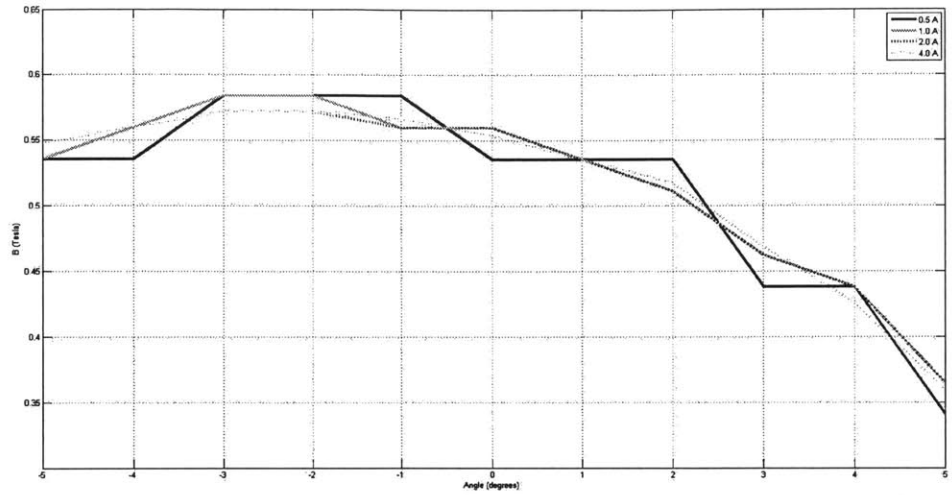

Figure 5.1: Effective magnetic field

As we saw in Chapter 3, the steepness of the actuator is largely dependent on the winding density. We were able to achieve an average steepness of around $S = 0.0012$. However, the same actuator, if wound with a density of unity, that is to say that the winding area was filled completely with windings, would have a steepness closer to twice that.

The discrepancy between the predicted value of S and the measured value can be attributed to the slightly lower B field, and our overly optimistic prediction (We assumed $B = 0.6T$ everywhere). It may be possible to improve performance by merely centering the coils more carefully as suggested by Figure 5.1

5.2 Conclusion of Thesis

In this thesis, a set of modular Lorentz force actuators was designed, manufactured and demonstrated. An automated design process was developed for rapid design iteration. Preliminary testing demonstrated adequate performance and modest efficiencies. Results were fairly consistent with design values, validating our process.

The prototype actuator design that we came up with met all of our initial design goals.

Our testing demonstrated that direct drive voice coil actuators could be used for distributed actuation of the RoboTuna.

Perhaps more useful than the prototypes themselves was the automated design process that we developed. The distributed nature of the flexible-hull RoboTuna demands many similar, yet scaled actuators. The script we developed allows a designer to easily adjust design parameters including dimensional constraints and analyze the resulting design almost instantaneously.

Further experiments could be done to better determine the mechanical load presented by the RoboTuna's tail and the required torques. Our design process could then be used to develop actuators that are optimized for each vertebra.

One key area for improvement of the current design is the coil winding process. Improvements in winding density could potentially double steepness, substantially increasing efficiency.

Our original analysis highlights the advantage of using an indirect drive train that effectively scales the mechanical load seen by the actuator. A pulse drive system could be used in conjunction with our actuators to achieve high efficiencies.

Appendix A

Matlab and Labview Code

Actuator_Gen_lib_2.m

```
function [possible_mags,Rank ] = Actuator_Gen_lib_1( xt,yt,zt,Halbach,hH,r,MAGNETS)
possible_mags=[];
index = 1;
openfemm
main_maximize
% xt - design within total x
% yt- and total y
% zt - depth into page
% hH -  height of Halbach
% Halbach - 1 for magnets, 0 for air
Br = 1.32;
Bg = .5*Br;
Bcsat = 1.5;            % more of a rough limit on Bc
magmargin = .02;
Am1 = (yt-(2*hH))/(1+(Bg/Bcsat));
Ac = (Bg/Bcsat)*Am1;
lm1 = (xt-Ac)/2;
ht = zt
Magx = lm1/2
Magy = Am1

for i = [1:length(MAGNETS)]             %Run through all the magnets
    currentmag = MAGNETS(i,:);
    for j = [1:3]                       %Try three rotations... and four configurations
        [xtT,ytT,ztT] = size_core(currentmag(1),currentmag(2),currentmag(3),hH);            %1*1*1
            if (xtT<=xt)&&(ytT<=yt)&&(ztT<=zt)
                    possible_mags(index,:) = currentmag;
                    index = index+1;
            end
        [xtT,ytT,ztT] = size_core(currentmag(1),2*currentmag(2),currentmag(3),hH);          %1*2*1
            if (xtT<=xt)&&(ytT<=yt)&&(ztT<=zt)
                    possible_mags(index,:) = [currentmag(1),2*currentmag(2),currentmag(3)];
                    index = index+1;
            end
        [xtT,ytT,ztT] = size_core(currentmag(1),2*currentmag(2),2*currentmag(3),hH);        %1*2*2
            if (xtT<=xt)&&(ytT<=yt)&&(ztT<=zt)
                    possible_mags(index,:) = [currentmag(1),2*currentmag(2),2*currentmag(3)];
                    index = index+1;
            end
            [xtT,ytT,ztT] = size_core(currentmag(1),currentmag(2),2*currentmag(3),hH);      %1*1*2
            if (xtT<=xt)&&(ytT<=yt)&&(ztT<=zt)
                    possible_mags(index,:) = [currentmag(1),currentmag(2),2*currentmag(3)];
                    index = index+1;
            end

      currentmag = circshift(currentmag,[0,1]);
    end
    currentmag = fliplr(currentmag);
    for j = [1:3]                       %and the other three,four
        [xtT,ytT,ztT] = size_core(currentmag(1),currentmag(2),currentmag(3),hH);            %1*1*1
            if (xtT<=xt)&&(ytT<=yt)&&(ztT<=zt)
                    possible_mags(index,:) = currentmag;
                    index = index+1;
```

```
        end
    [xtT,ytT,ztT] = size_core(currentmag(1),2*currentmag(2),currentmag(3),hH);          %1*2*1
        if (xtT<=xt)&&(ytT<=yt)&&(ztT<=zt)
                possible_mags(index,:) = [currentmag(1),2*currentmag(2),currentmag(3)];
                index = index+1;
        end
    [xtT,ytT,ztT] = size_core(currentmag(1),2*currentmag(2),2*currentmag(3),hH);        %1*2*2
        if (xtT<=xt)&&(ytT<=yt)&&(ztT<=zt)
                possible_mags(index,:) = [currentmag(1),2*currentmag(2),2*currentmag(3)];
                index = index+1;
        end
        [xtT,ytT,ztT] = size_core(currentmag(1),currentmag(2),2*currentmag(3),hH);      %1*1*2
        if (xtT<=xt)&&(ytT<=yt)&&(ztT<=zt)
                possible_mags(index,:) = [currentmag(1),currentmag(2),2*currentmag(3)];
                index = index+1;
        end
  currentmag = circshift(currentmag,[0,1]);
 end
end
Rank = (possible_mags(:,1).*possible_mags(:,2).*possible_mags(:,3))/(Am1*lm1*zt);
[C,I] = max(Rank)
bestbet = possible_mags(I,:)
lm = 2*possible_mags(I,(1))
Am = possible_mags(I,(2))
zt = possible_mags(I,(3))
 [xt,yt,zt] = size_core(possible_mags(I,(1)),possible_mags(I,(2)),possible_mags(I,(3)),hH)
% Am = (yt-(2*hH))/(1+(Bg/Bcsat));
Ac = (Bg/Bcsat)*Am;
% lm = (xt-Ac)/2;

create(0)               % create a new magnetics problem
%%%%%%%%%%%%%%%
%Get Materials%
%%%%%%%%%%%%%%%
mi_getmaterial('Air');
mi_getmaterial('NdFeB 40 MGOe');
mi_getmaterial('Pure Iron');

%%%%%%%%%%%%%%%%
%Set Boundaries%
%%%%%%%%%%%%%%%%
mi_drawarc(0,-4,0,4,180,1);
mi_drawarc(0,4,0,-4,180,1)
mi_addboundprop('ABC',0,0,0,0,0,0,80850.71109068283,0,2);
mi_selectarcsegment(4,0);
mi_setarcsegmentprop(1,'ABC',0,0);
mi_selectarcsegment(-4,0);
mi_setarcsegmentprop(1,'ABC',0,0);

%%%%%%%%%%%%%%%%%%%%%%%%%%%
%draw outer edge of iron%
%%%%%%%%%%%%%%%%%%%%%%%%%%%
x_oc1 = xt/2;
y_oc1 = yt/2;
x_oc2 = -x_oc1;
y_oc2 = -y_oc1;
mi_drawrectangle(x_oc1-(xt/2),y_oc1,x_oc2-(xt/2),y_oc2)
mi_addblocklabel(x_oc1-.01-(xt/2),y_oc1-.01);
mi_selectlabel(x_oc1-.01-(xt/2),y_oc1-.01);
mi_setblockprop('Pure Iron',1,.01,0,0,0,0);
mi_clearselected;
mi_addblocklabel(x_oc1+.05-(xt/2),y_oc1+.05);
mi_selectlabel(x_oc1+.05-(xt/2),y_oc1+.05);
mi_setblockprop('Air',1,.01,0,0,0,0);
mi_clearselected;
mi_drawrectangle(x_oc1+(xt/2),y_oc1,x_oc2+(xt/2),y_oc2)
mi_addblocklabel(x_oc1-.01+(xt/2),y_oc1-.01);
mi_selectlabel(x_oc1-.01+(xt/2),y_oc1-.01);
mi_setblockprop('Pure Iron',1,.01,0,0,0,0);
mi_clearselected;

%%%%%%%%%%%%%%%%%%%%%%%%%%%
%draw inner edge of iron%
%%%%%%%%%%%%%%%%%%%%%%%%%%%
x_ic1 = (xt-Ac)/2;
y_ic1 = (yt-Ac)/2;
x_ic2 = -x_ic1;
y_ic2 = -y_ic1;
mi_drawrectangle(x_ic1+(xt/2),y_ic1,x_ic2+(xt/2),y_ic2)
mi_drawrectangle(x_ic1-(xt/2),y_ic1,x_ic2-(xt/2),y_ic2)
%%%%%%%%%%%%%%%
%draw magnets%
%%%%%%%%%%%%%%%
x_lm1 = x_ic1;
y_lm1 = y_ic1-hH;
x_lm2 = x_ic1-(lm/2);
y_lm2 = -y_lm1;
mi_drawrectangle(x_lm1+(xt/2),y_lm1,x_lm2+(xt/2),y_lm2)          %Right
mi_drawrectangle(-x_lm1+(xt/2),y_lm1,-x_lm2+(xt/2),y_lm2)        %Left
mi_addblocklabel(((x_lm1+x_lm2)/2)+(xt/2),(y_lm1+y_lm2)/2);
mi_selectlabel(((x_lm1+x_lm2)/2) +(xt/2),(y_lm1+y_lm2)/2);
mi_setblockprop('NdFeB 40 MGOe',1,.01,0,0,0,0);
mi_clearselected;
mi_addblocklabel((-(x_lm1+x_lm2)/2)+(xt/2),(y_lm1+y_lm2)/2);
mi_selectlabel((-(x_lm1+x_lm2)/2)+(xt/2),(y_lm1+y_lm2)/2);
```

```
mi_setblockprop('NdFeB 40 MGOe',1,.01,0,0,0,0);
mi_clearselected;
mi_drawrectangle(x_lm1-(xt/2),y_lm1,x_lm2-(xt/2),y_lm2)          %Right
mi_drawrectangle(-x_lm1-(xt/2),y_lm1,-x_lm2-(xt/2),y_lm2)        %Left
mi_addblocklabel(((x_lm1+x_lm2)/2 )-(xt/2),(y_lm1+y_lm2)/2);
mi_selectlabel(((x_lm1+x_lm2)/2) -(xt/2),(y_lm1+y_lm2)/2);
mi_setblockprop('NdFeB 40 MGOe',1,.01,0,180,0,0);
mi_clearselected;
mi_addblocklabel((-(x_lm1+x_lm2)/2)-(xt/2),(y_lm1+y_lm2)/2);
mi_selectlabel((-(x_lm1+x_lm2)/2)-(xt/2),(y_lm1+y_lm2)/2);
mi_setblockprop('NdFeB 40 MGOe',1,.01,0,180,0,0);
mi_clearselected;
%%%%%%%%%%%%%%%%%%%%%%%%%%%%%%%%
%draw Halbach/side clearances%
%%%%%%%%%%%%%%%%%%%%%%%%%%%%%%%%
if hH>0
x_hH1 = x_ic1;
y_hH1 = y_ic1;
x_hH2 = x_ic1-(lm/2);
y_hH2 = y_ic1-hH;
mi_drawrectangle(x_hH1+(xt/2),y_hH1,x_hH2+(xt/2),y_hH2);         %Upper Right
mi_drawrectangle(-x_hH1+(xt/2),y_hH1,-x_hH2+(xt/2),y_hH2);          %Upper Left
mi_drawrectangle(x_hH1+(xt/2),-y_hH1,x_hH2+(xt/2),-y_hH2);          %Lower Right
mi_drawrectangle(-x_hH1+(xt/2),-y_hH1,-x_hH2+(xt/2),-y_hH2);          %Lower Left

mi_drawrectangle(x_hH1-(xt/2),y_hH1,x_hH2-(xt/2),y_hH2);         %Upper Right
mi_drawrectangle(-x_hH1-(xt/2),y_hH1,-x_hH2-(xt/2),y_hH2);          %Upper Left
mi_drawrectangle(x_hH1-(xt/2),-y_hH1,x_hH2-(xt/2),-y_hH2);          %Lower Right
mi_drawrectangle(-x_hH1-(xt/2),-y_hH1,-x_hH2-(xt/2),-y_hH2);          %Lower Left

if Halbach == 0
    mat_h = 'Air';
else
    mat_h = 'NdFeB 40 MGOe';
end
mi_addblocklabel((x_hH1+x_hH2)/2 +(xt/2),(y_hH1+y_hH2)/2);  %Upper Right
mi_selectlabel((x_hH1+x_hH2)/2 +(xt/2),(y_hH1+y_hH2)/2);
mi_setblockprop(mat_h,1,.01,0,90,0,0);
mi_clearselected;
mi_addblocklabel(-(x_hH1+x_hH2)/2 +(xt/2),(y_hH1+y_hH2)/2); %Upper Left
mi_selectlabel(-(x_hH1+x_hH2)/2 +(xt/2),(y_hH1+y_hH2)/2);
mi_setblockprop(mat_h,1,.01,0,-90,0,0);
mi_clearselected;
mi_addblocklabel((x_hH1+x_hH2)/2 +(xt/2),-(y_hH1+y_hH2)/2);   %Lower Right
mi_selectlabel((x_hH1+x_hH2)/2 +(xt/2),-(y_hH1+y_hH2)/2);
mi_setblockprop(mat_h,1,.01,0,-90,0,0);
mi_clearselected;
mi_addblocklabel(-(x_hH1+x_hH2)/2 +(xt/2),-(y_hH1+y_hH2)/2);     %Lower Left
mi_selectlabel(-(x_hH1+x_hH2)/2 +(xt/2),-(y_hH1+y_hH2)/2);
mi_setblockprop(mat_h,1,.01,0,90,0,0);
mi_clearselected;
mi_addblocklabel((x_hH1+x_hH2)/2 -(xt/2),(y_hH1+y_hH2)/2);  %Upper Right
mi_selectlabel((x_hH1+x_hH2)/2 -(xt/2),(y_hH1+y_hH2)/2);
mi_setblockprop(mat_h,1,.01,0,-90,0,0);
mi_clearselected;
mi_addblocklabel(-(x_hH1+x_hH2)/2 -(xt/2),(y_hH1+y_hH2)/2); %Upper Left
mi_selectlabel(-(x_hH1+x_hH2)/2 -(xt/2),(y_hH1+y_hH2)/2);
mi_setblockprop(mat_h,1,.01,0,90,0,0);
mi_clearselected;
mi_addblocklabel((x_hH1+x_hH2)/2 -(xt/2),-(y_hH1+y_hH2)/2);   %Lower Right
mi_selectlabel((x_hH1+x_hH2)/2 -(xt/2),-(y_hH1+y_hH2)/2);
mi_setblockprop(mat_h,1,.01,0,90,0,0);
mi_clearselected;
mi_addblocklabel(-(x_hH1+x_hH2)/2 -(xt/2),-(y_hH1+y_hH2)/2);     %Lower Left
mi_selectlabel(-(x_hH1+x_hH2)/2 -(xt/2),-(y_hH1+y_hH2)/2);
mi_setblockprop(mat_h,1,.01,0,-90,0,0);
mi_clearselected;

end
% if Halbach==2
%
%     mi_drawrectangle(x_hH2,y_hH1,-x_hH2,y_hH2);
%
%     mi_drawrectangle(x_hH2,-y_hH1,-x_hH2,-y_hH2);
%
%     mi_addblocklabel(0,(y_hH1+y_hH2)/2);
%     mi_selectlabel(0,(y_hH1+y_hH2)/2);
%     mi_setblockprop(mat_h,1,.01,0,180,0,0);       %see page 5
%     mi_clearselected;
%
%     mi_addblocklabel(0,-(y_hH1+y_hH2)/2);
%     mi_selectlabel(0,-(y_hH1+y_hH2)/2);
%     mi_setblockprop(mat_h,1,.01,0,180,0,0);       %see page 5
%     mi_clearselected;
% end
%%%%%%%%%%%%%%%%%%%%%%%%%%%%
%draw winding%
%%%%%%%%%%%%%%%%%%%%%%%%%%%%
arclength = 12*(2*pi/360)*r %tan(...(r-(Ac+lm)/2));
x_w1 = (lm/2)-magmargin;
y_w1 = (Am - arclength)/2;
x_w2 = -x_w1;
y_w2 = -y_w1;
mi_drawrectangle(x_w1+(xt/2),y_w1,x_w2+(xt/2),y_w2)
mi_addblocklabel((xt/2),0);
```

```
mi_selectlabel((xt/2),0);
mi_setblockprop('Air',1,.01,0,0,0,0);
mi_clearselected;

mi_drawrectangle(x_w1-(xt/2),y_w1,x_w2-(xt/2),y_w2)
mi_addblocklabel(-(xt/2),0);
mi_selectlabel(-(xt/2),0);
mi_setblockprop('Air',1,.01,0,0,0,0);
mi_clearselected;

%Center is Air:
mi_addblocklabel((xt/2),y_ic1-.05);
mi_selectlabel((xt/2),y_ic1-.05);
mi_setblockprop('Air',1,.01,0,0,0,0);
mi_clearselected;
mi_addblocklabel(-(xt/2),y_ic1-.05);
mi_selectlabel(-(xt/2),y_ic1-.05);
mi_setblockprop('Air',1,.01,0,0,0,0);       %see page 5
mi_clearselected;

mi_zoomnatural
mi_probdef(0,'inches','planar',1e-8,zt,30,0)
mi_saveas('half_half_1_1.fem')
mi_analyze
mi_loadsolution
mo_zoomnatural
mo_showdensityplot(1,0,1.5,0,'mag')
mo_addcontour((xt/2),y_lm1)
mo_addcontour((xt/2),y_lm2)
mo_makeplot(2,200)

ht = zt;
Magx = lm/2;
Magy = Am;

Hhx = Am;
Hhy = hH;
Corey1=Ac/2;
Corey2= yt-(Ac/2);
Corexo= 2*xt;
Corexi= 2*lm;
CoreA = Ac/2;

Wirex = x_w1*2;
Wirey = y_w1*2;
filepath = sprintf('C:\\Users\\jcchurch\\Dropbox\\TUNA\\Actuator Solidworks\\Rev_1\\equations.txt')

fileID = fopen(filepath,'w');

fprintf(fileID,'%6s = %12.8f \r\n','ht',ht);
fprintf(fileID,'%6s = %12.8f \r\n','Magx',Magx);
fprintf(fileID,'%6s = %12.8f \r\n','Magy',Magy);
fprintf(fileID,'%6s = %12.8f \r\n','Hhx',Hhx);
fprintf(fileID,'%6s = %12.8f \r\n','Hhy',Hhy);
fprintf(fileID,'%6s = %12.8f \r\n','Corey1',Corey1);
fprintf(fileID,'%6s = %12.8f \r\n','Corey2',Corey2);
fprintf(fileID,'%6s = %12.8f \r\n','Corexo',Corexo);
fprintf(fileID,'%6s = %12.8f \r\n','Corexi',Corexi);
fprintf(fileID,'%6s = %12.8f \r\n','CoreA',CoreA);
fprintf(fileID,'%6s = %12.8f \r\n','Wirex',Wirex);
fprintf(fileID,'%6s = %12.8f \r\n','Wirey',Wirey);
fprintf(fileID,'%6s = %12.8f \r\n','xt',xt);
fprintf(fileID,'%6s = %12.8f \r\n','yt',yt);
fprintf(fileID,'%6s = %12.8f \r\n','magmargin',magmargin);
type(filepath)
fclose(fileID);
end
```

Labview Code

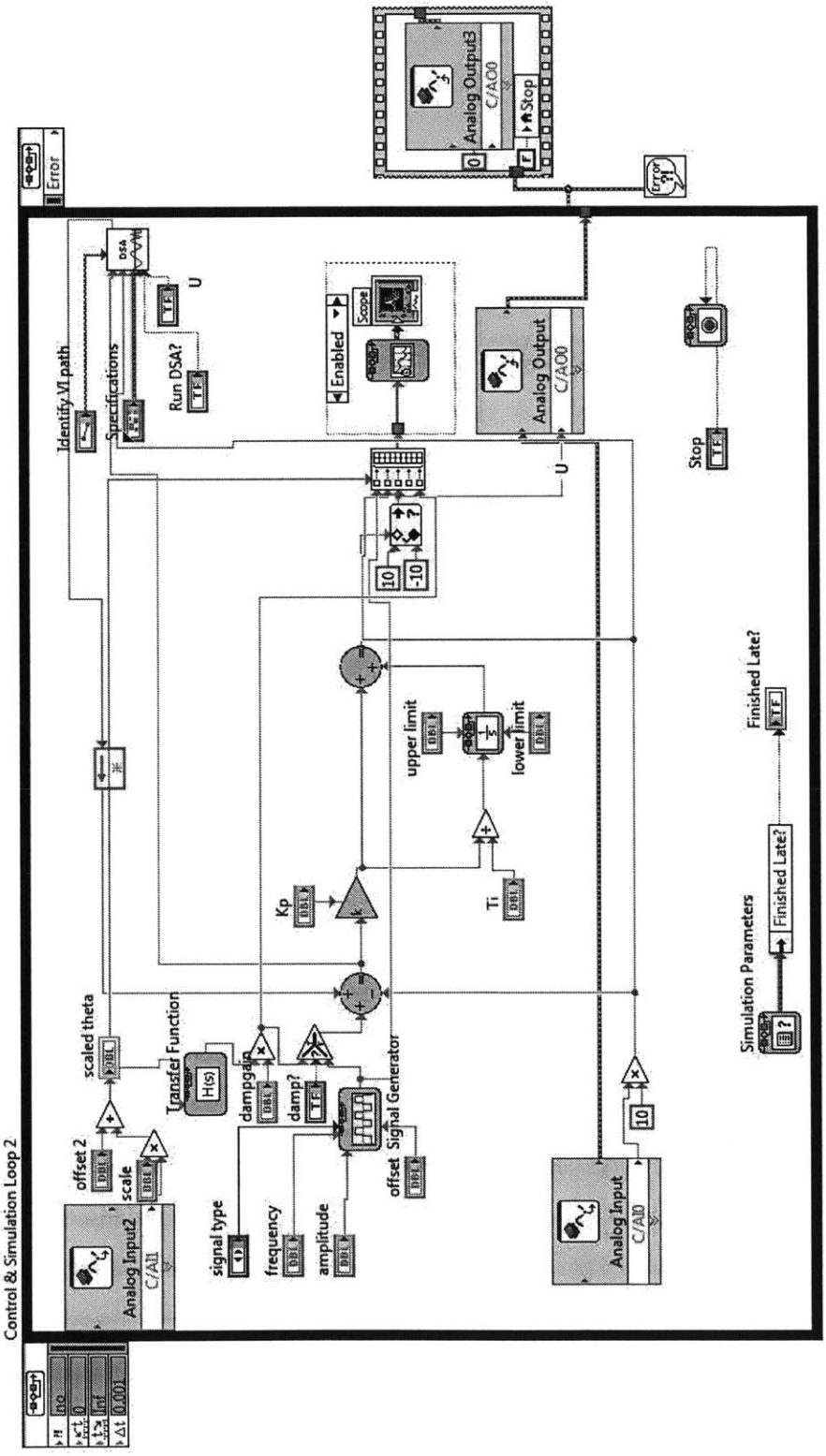

Bibliography

[1] David Scott Barrett. *Propulsive Efficiency of a Flexible Hull Undersea Vehicle.* PhD thesis, 1994.

[2] Lih-Chung Chang, Hai-Chau; Wang. A simple proof of thue's theorem on circle packing.

[3] A. Pressman et al. *Switching Power Suppy Design.* McGraw-Hill.

[4] 2013 Finite Element Method Magnetics. http://www.femm.info/wiki/homepage.

[5] Jeroen Scholten. Modelling of direct drive motors for performance improvement by design and control, October 2004.

[6] Zhen Sun. High efficiency pulse motor drive for robotic propulsion. Master's thesis, Massachusetts Institute of Technology, Cambridge, MA, 2013.